Tellus (1999), 51A, 686–697
Printed in UK – all rights reserved

TELLUS
ISSN 0280–6495

The genesis and predictability of persistent Pacific–North American anomalies in a model atmosphere

By HAI LIN* and JACQUES DEROME, *Department of Atmospheric and Oceanic Sciences and Centre for Climate and Global Change Research, McGill University, 805 Sherbrooke Street West, Montréal, Québec H3A 2K6, Canada*

(Manuscript received 7 September 1998; in final form 11 January 1999)

ABSTRACT

The setup process of Pacific–North American (PNA) pattern anomalies that last more than 10 days and the role played therein by synoptic-scale transients are investigated using a T21, 3-level quasi-geostrophic model. As there is no time-dependent forcing in the model, the low-frequency PNA anomalies are generated entirely by the internal dynamics. From a 300-winter integration, 100 cases of positive PNA anomalies and 118 cases of negative PNA anomalies lasting at least 10 days are identified. The PNA composites reveal that 5 days before the setup of a positive (negative) PNA anomaly there is a negative (positive) height anomaly over Canada. This anomaly moves westward and stops over the North Pacific. It then intensifies and a wave train develops downstream. The rôle played by the synoptic-scale transients is explored by prediction experiments starting from day -5 (5 days before the appearance of a PNA anomaly). A 5-day average centered at day -5 is used to remove the synoptic-scale transients from the initial state. The results indicate that even without these transients in the initial conditions, the setup process of a positive PNA anomaly can be reproduced quite well. On the other hand, the setup of a negative PNA pattern cannot be predicted if the synoptic-scale transients are absent from the initial conditions. In this case, the pattern evolves systematically, but differently from the way it evolves in the control run.

1. Introduction

There have been a great number of studies on the atmospheric low-frequency variabilities, which have time scales beyond the synoptic scale of about a week, as summarized by Pandolfo (1993). In contrast to the synoptic-scale eddies, whose three-dimensional structure and time evolution are reasonably well understood, the dynamics of the low-frequency variabilities are less clear. One of the important processes in the dynamics of the low-frequency variabilities is the interaction with the baroclinic synoptic-scale transients. The synoptic-scale eddies interact with the low-frequency fluctuations through their transports of vorticity and heat. The importance of the "transient forcing" to the low-frequency variability has been shown in several studies (Green, 1977; Mullen, 1987; Klasa et al., 1992). Other possible mechanisms for the generation of low-frequency variabilities include the instability of the zonally-varying climatological basic state (Simmons et al., 1983; Frederiksen, 1979), and some forcing from the lower boundary (Horel and Wallace, 1981).

It would be of interest to determine which, if any, of the above mechanisms dominates in different circumstances — the high-frequency eddy forcing, the instability of the background state or the external forcing. If one of the latter two is totally dominant, the evolution of the atmosphere in a numerical forecast would be relatively insensitive to the details of the representation of the baroclinic

* Corresponding author.

eddies in the initial conditions. Kushnir and Wallace (1989) looked into this problem by conducting forecast experiments after removing the baroclinic waves in the initial conditions. Their results show that the low-frequency components of the flow are affected differently depending on their zonal scales, i.e., waves of wavenumbers 1–3 are only weakly affected by the removal of the synoptic eddies in the initial conditions, while waves of wavenumbers 4–6 tend to drift eastward erroneously.

In the present study, we concentrate on a special case of the low-frequency variability — the Pacific–North American (PNA) anomalies that last more than 10 days. The objective is to analyze the time evolution of the setup process of these anomalies and to investigate the importance of the high-frequency eddies in their genesis. To see the sensitivity of the evolution of the PNA to the representation of the baroclinic eddies in the initial conditions, an approach similar to that of Kushnir and Wallace (1989) is used, i.e., we examine the consequences of removing the high-frequency part of the flow in the initial conditions in a numerical forecast. We compare the two opposite phases of the PNA to assess the predictability of the genesis of the PNA and its dependence on its phase.

The association between the phase of mean-seasonal PNA anomalies and the transient activity has been presented by Lin and Derome (1997) using observations, and by Lin and Derome (1996) using a 3-level model. The transient eddy activity was found to be substantially weaker in the North Pacific during a positive PNA than that during a negative PNA. In other words, relatively strong transient activity coexists with a negative PNA, while a positive PNA is associated with relatively weak eddies in the North Pacific. Does a negative PNA rely more on the transients than a positive PNA? If that is the case, removing high-frequency eddies in the initial conditions would have a bigger impact on the prediction of a negative PNA than on the forecast of a positive PNA. We will examine this aspect in the following sections.

The PNA pattern normally refers to an anomaly observed in mean-monthly or mean-seasonal data. In the present study we will examine PNA anomalies with shorter time scales, in that we consider those that have a significant amplitude for at least 10 consecutive days. We will focus on the several days around the onset of the persistent PNA anomalies.

2. The model and control run

The model used in this study is the spectral three level quasi-geostrophic (QG) model of Marshall and Molteni (1993). It has a global domain with pressure as the vertical coordinate and the horizontal resolution is triangular 21 (T21). The prognostic equations for the quasi-geostrophic potential vorticity are written at 200, 500 and 800 hPa as:

$$\frac{\partial q_i}{\partial t} = -J(\psi_i, q_i) - D_i + F_i, \tag{1}$$

where the index $i = 1$, 2 or 3 indicates the 200, 500 and 800 hPa pressure levels, respectively. The potential vorticity is defined as:

$$q_1 = \nabla^2\psi_1 - R_1^{-2}(\psi_1 - \psi_2) + f,$$
$$q_2 = \nabla^2\psi_2 + R_1^{-2}(\psi_1 - \psi_2) - R_2^{-2}(\psi_2 - \psi_3) + f,$$
$$q_3 = \nabla^2\psi_3 + R_2^{-2}(\psi_2 - \psi_3) + f\left(1 + \frac{h}{H_0}\right),$$

where $f = 2\Omega \sin\phi$, $R_1(= 700\ \mathrm{km})$ and $R_2(= 450\ \mathrm{km})$ are the Rossby radii of deformation for the 200–500 hPa layer and the 500–800 hPa layer, respectively. h is the orographic height and H_0 a scale height (9 km).

The dissipative terms D_1, D_2, and D_3 include the effects of a Newtonian relaxation of temperature, linear drag on the 800 hPa wind, and horizontal diffusion of vorticity and temperature. The terms F_1, F_2, and F_3 are time independent but spatially varying sources of potential vorticity. As suggested by Roads (1987), they can be determined by requiring that in (1) the potential vorticity tendency terms vanish for a long time average of observations, i.e.,

$$-\overline{J(\psi, q)} - \overline{D(\psi)} + F = 0, \tag{2}$$

where the overbar represents a time average, and the vertical index is omitted for simplicity. If $\psi_c = \bar{\psi}$ is the observed climatological mean, and a prime denotes a deviation from the mean, (2) can be rewritten as:

$$-J(\psi_c, q_c) - \overline{J(\psi', q')} - D(\psi_c) + F = 0, \tag{3}$$

where $J' = -\overline{J(\psi', q')}$ is the contribution of transients to the average potential vorticity tendency. As in some barotropic models (Simmons et al., 1983), one way to obtain the forcing field is to neglect the term J'. This assumes that the observed climatology is an exact stationary solution, and the role of transients that strongly contribute to the generation and maintainance of the mean itself is totally ignored. Here we follow Roads (1987) and calculate F using (3) with J' included. The model then will generate a mean state identical to ψ_c only if its internal variability is equal to the observed one in the sense that its J' equals that calculated from observations. As discussed by Lin and Derome (1996), the model used in this study is able to reproduce remarkably realistic stationary planetary waves and the broad climatological characteristics of the transients are in general agreement with observations.

The daily (12 GMT) European Centre for Medium Range Weather Forecasts (ECMWF) analyses for a period of 9 winter seasons from 1980/81 to 1988/89 are used, where the winter is defined as December, January and February. F is calculated using (3) for each winter, and the average for nine winters is used for the model. Therefore, transients with periods shorter than 90 days are included in the calculation of J', and hence of F.

With the external forcing obtained from the winter observations, a perpetual winter integration is performed. After an initial spin-up period of 360 days, model output data are saved once per day for 31,485 days. These 31,485 days are divided into 300 independent winters of 90 days by omitting the 15 days between consecutive 90 day periods. Thus in the following analysis 27,000 days of model data are used. The long-time integration will serve as a reference atmospheric state, and will be referred to as the control run. An analysis is conducted on the reference state to study the genesis process of the PNA patterns in the model. It is against this reference state that all predictability experiments discussed in the later sections will be compared. The model output in streamfunction is converted into geopotential height using the linear balance equation. The output Gaussian grid data are converted to latitude-longitude grid data with a resolution of $5° \times 5°$. In the following discussion we will focus on the 500 hPa geopotential height field north of 20°N.

3. Set-up process of the PNA patterns

With a time-independent forcing, we are dealing with variabilities that are entirely internally generated by the model's dynamics. One of the most significant low-frequent fluctuation patterns in the atmosphere and in the model is the PNA (Wallace and Gutzler, 1981; Corti and Palmer, 1997). To describe the time evolution of the PNA, a daily PNA index is calculated from the model's 500 hPa geopotential height output, following Wallace and Gutzler (1981):

$$\begin{aligned}\text{PNA index}\\ &= \tfrac{1}{4}[z'(20°\text{N}, 160°\text{W}) - z'(45°\text{N}, 165°\text{W})\\ &\quad + z'(55°\text{N}, 115°\text{W}) - z'(30°\text{N}, 85°\text{W})], \quad (4)\end{aligned}$$

where z' represents a departure of a particular day from the model's climatological 500 hPa height for that grid point, normalized by the local standard deviation of that departure. The positive (negative) PNA index is associated with negative (positive) height anomalies over the North Pacific and the southeastern USA and positive (negative) height anomalies over Hawaii and western Canada.

The daily PNA index is then low-pass filtered to remove the effects of the brief transient fluctuations associated with the passage of synoptic-scale disturbances. That is accomplished with a Fourier filter that removes the high-frequency (shorter than 10 days) signal, and is applied to the daily time series of the PNA index for every 90-day winter. The transients kept in the PNA index thus have time scales from 10 to 90 days. A persistent positive (negative) PNA anomaly is said to occur when the index remains equal to or greater (less) than a specified threshold value M $(-M)$ for at least L days. M is chosen to be 0.4σ, where σ is the standard deviation of the filtered PNA index, and L is set to 10 days. Another condition for choosing the persistent anomaly cases is that the beginning of a selected case has to occur at least 10 days after the end of the previous case or the first day of the winter. As we will perform prediction experiments for the onset of the PNA, we do not want to start a forecast from an existing PNA pattern. In this way, from the data of 300 winters, we have selected 100 positive PNA cases and 118 negative PNA cases. The duration for the selected cases ranges from 10 to 25 days, with an average of 14 days.

A reference day (day 0) is defined for every case as the first day when the PNA index crosses the amplitude threshold. To demonstrate the evolution of the PNA onset, composites are made separately for both the positive and negative persistent PNA anomalies starting from a few days before day 0. A student *t*-test for significantly different means between the composite and the climatology is conducted. Fig. 1 shows the setup process of the positive PNA from day −5 to day 3, which is the composite of 500 hPa geopotential height anomalies (departure from the model climatology) of the 100 selected cases. Areas with statistical significance over the 99% level are shaded. Five days before the set-up of a positive PNA anomaly (Fig. 1a), a weak pattern with some similarity to a negative PNA is observed, which has a positive height anomaly centre over the North Pacific and a negative one over western Canada. The maximum amplitude is about 40 m. With time the negative anomaly centre over western Canada moves southwestward and intensifies

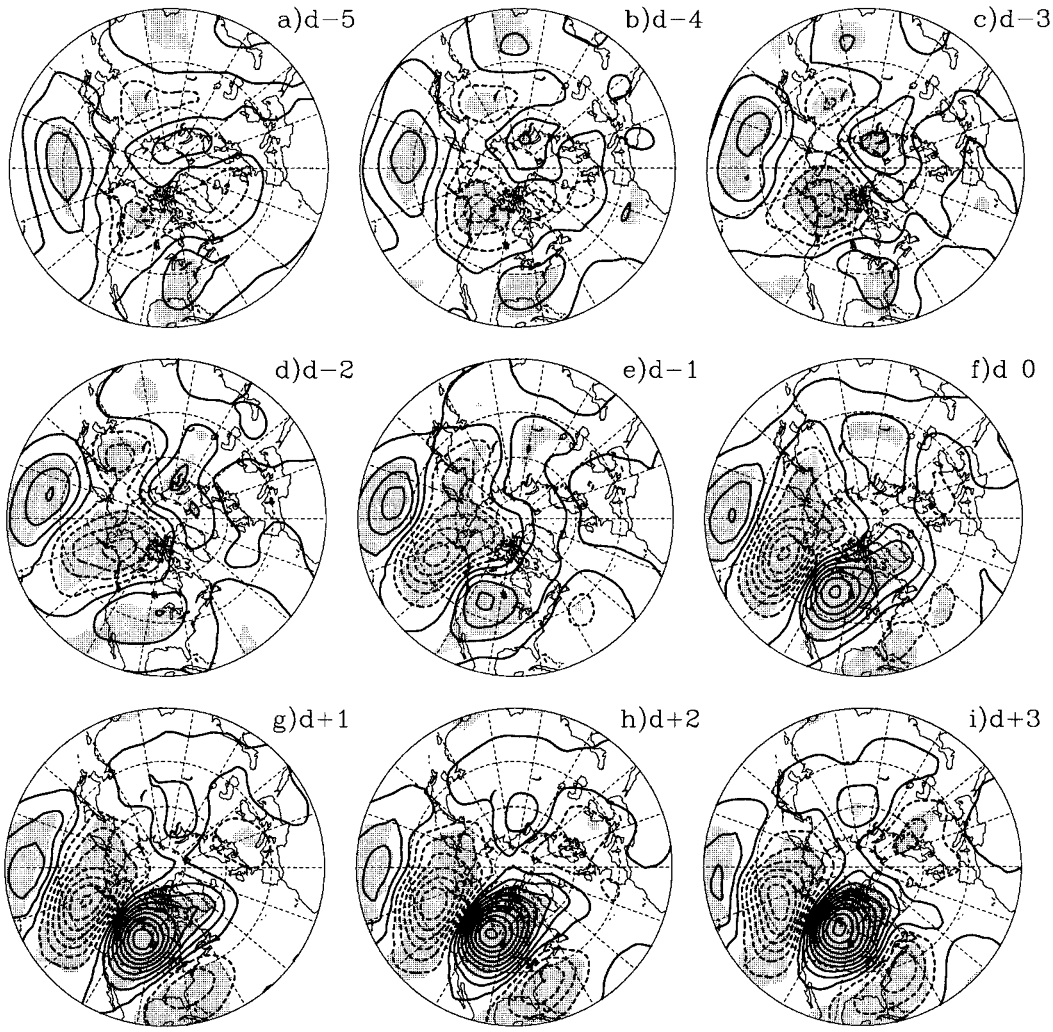

Fig. 1. Time evolution of positive PNA genesis from day −5 to day 3 by compositing 100 cases in the control run. Contour interval is 20 m. Areas with significance level over 99% are shaded.

until it reaches about 45°N, 160°W. The positive anomaly centre in the North Pacific is seen to move to the south. At the same time, a ridge develops over the southeastern Unites States and moves northwestwards. By day 0 (Fig. 1f), a well organized positive PNA pattern has been developed. Thereafter, the pattern remains nearly stationary, and some evidence of a downstream development by energy dispersion can be observed.

The development of the negative PNA pattern is illustrated in Fig. 2, which is the composite of the 500 hPa geopotential height anomaly of 118 negative PNA cases. As in the case of the positive PNA composite, but opposite in sign, we see a significant positive height anomaly centre over western Canada five days before the setup of the negative PNA (Fig. 2a). In contrast to the positive PNA onset at day -5, the height anomaly distribution shows little signature of a positive PNA. The positive height anomaly centre over western Canada undergoes a similar evolution as the negative centre in the positive PNA case, i.e., it slowly moves southwestward and intensifies until it reaches about 45°N, 160°W. A fully developed negative PNA is seen on day 0. Downstream

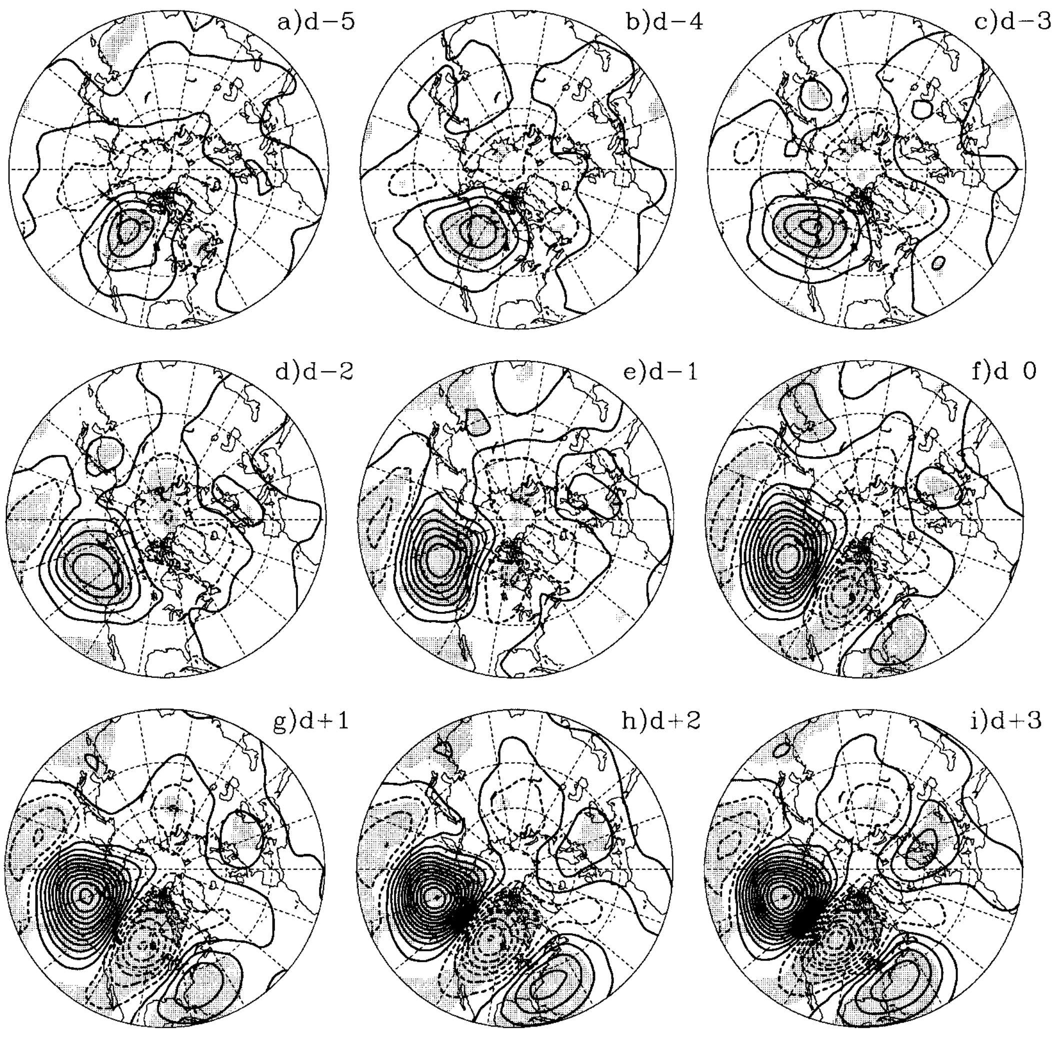

Fig. 2. Same as Fig. 1, but for negative PNA by compositing 118 cases.

development by energy dispersion is even clearer than in the positive PNA case.

In a series of papers, Dole and colleagues (Dole and Gordon, 1983; Dole, 1986) documented the characteristics of persistent height anomalies over the wintertime Northern Hemisphere. The persistent anomalies were selected as those for which the 500 hPa height anomaly satisfied threshold and duration criteria of ± 100 m and 10 days, respectively. One of the key regions they identified as having a high number of persistent anomalies is the North Pacific near 45°N, 170°W. A composite time evolution for the onset of the anomalies was constructed by averaging over all case evolutions relative to the time when the anomaly magnitude first exceeds 100 m at the reference point. The results show little evidence of a precursor until a few days prior to the onset (Dole, 1986). During the onset of the composite North Pacific persistent anomaly, a wave train emanating from the key region, develops with little sign of phase propagation.

Instead of using the height anomaly at a reference (key) point, we used the daily PNA index to define the onset of the low-frequency pattern over the Pacific and North American regions. The time series of the PNA index and the height anomaly at the North Pacific key point used by Dole (1986) (45°N, 170°W) are strongly correlated. Our definition is less localized than Dole's and represents the most significant wintertime anomaly pattern over the Northern Hemisphere. In Dole (1986), observational data of 14 winters were used, and only 15 positive and 13 negative cases were selected according to the height anomaly at the key point. In the present study, the use of a Q–G model allows us to generate a longer record of winter data, with 100 positive and 118 negative PNA cases, and hence to obtain results with a high statistical significance. The time-independent forcing in the model also allows us to isolate the internal dynamics as the only source of variability.

In contrast to Dole's (1986) life cycle composite of the North Pacific persistent anomalies, which showed little evidence of a precursor before the onset, the present analysis of the three-level Q–G model output shows a significant signal five days before the onset of the PNA pattern. We have seen that a negative (positive) height anomaly over Canada 5 days prior to the onset of a positive (negative) PNA moves southwestward and stops over the North Pacific. It then intensifies and a wave train develops downstream.

4. Prediction experiments

For every positive and negative PNA case, a forecast is conducted starting from day -5 (5 days before its onset). Our goal is to examine the importance of the high-frequency eddies in the genesis of the PNA. Following Kushnir and Wallace (1989), the initial state is obtained by a 5-day average of the streamfunction fields of the control run centred at day -5. This initial state thus contains only the slowly varying part of the atmospheric flow at that time. This modification of the initial state can be viewed as an injection of errors in the initial conditions for the time integrations, errors that have a short time scales and hence can be expected to have short space scales. By looking at the growth rate of the errors we can assess the contribution of the high-frequency eddies to the forecast errors. Specifically, we will see if the generation process of the PNA pattern can be reproduced when the high-frequency transients are removed from the initial state.

Composites were made for the forecasts of both the positive and negative PNA cases. Fig. 3 shows the evolution of the flow for the forecast of the positive PNA, which is the composite of the predicted 500 hPa geopotential height anomalies of the 100 selected cases. Again, areas with statistical significance over the 99% level estimated by a student *t*-test are shaded. The evolution of the forecast height anomaly compares very well with that in the control run (Fig. 1). At day -5 a weak pattern similar to a negative PNA appears with a negative height anomaly over western Canada and a positive height anomaly over the North Pacific. This pattern is the low-pass filtered version of Fig. 1a. The negative anomaly over Canada moves southwestward and intensifies. The other centres also move with the negative centre upstream. By day -2, significant height anomalies have developed, and a positive phase PNA is formed, thereafter the centres intensify with little evidence of phase propagation. Despite the removal of high-frequency eddies in the initial condition, the weak negative PNA with a negative height anomaly centre over Canada at day -5 evolves into a

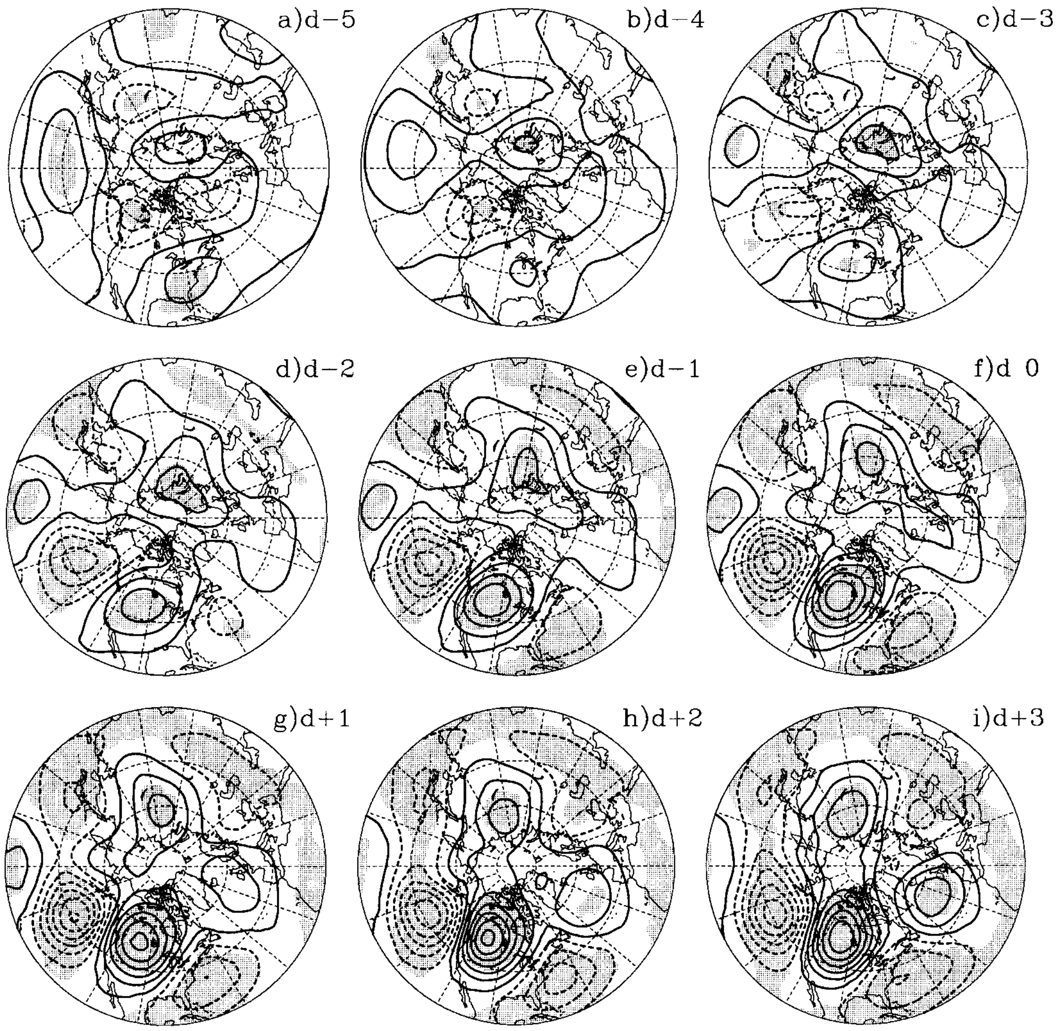

Fig. 3. Same as Fig. 1, but for prediction.

strong positive PNA pattern in a very similar way as in the control run.

The time evolution of the height anomaly composite of the negative PNA forecasts is presented in Fig. 4. The composite contains the predictions of the 118 negative PNA cases. We see that the pattern of evolution is very different from that of the control run. The initial positive height anomaly over western Canada at day −5 shows little signature of a southwestward movement during the following two days. Instead, at day −3, a zonal extension of the positive anomaly along about 60°N to the west across the North Pacific can be observed. At the same time, a zonally-elongated negative height anomaly forms in the central Pacific south of 40°N. In the following days the main centre of the positive height anomaly originally located in western Canada continues moving westward. A north–south dipole structure emerges in the Pacific with a zonally elongated positive height anomaly to the north and negative anomaly to the south. The two centres intensify and move slowly westward. By day 2 the height anomaly pattern is strongly reminiscent of the western Pacific (WP) pattern (Wallace and Gutzler, 1981).

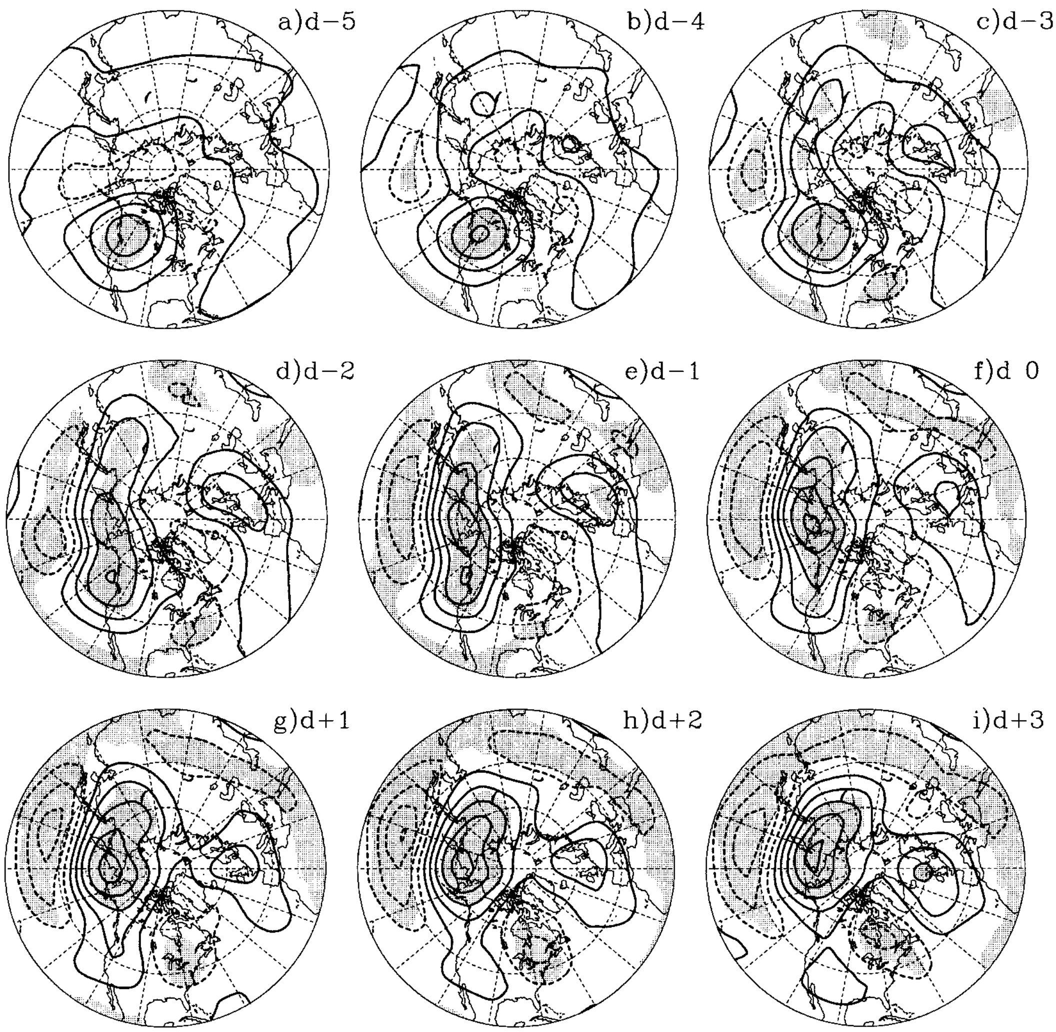

Fig. 4. Same as Fig. 2, but for prediction.

In summary, we have found that the effect of removing the baroclinic transients on the positive PNA generation process is different from that on the negative PNA setup. The genesis of a positive PNA is not sensitive to the details of the representation of the high-frequency eddies in the initial conditions, whereas the removal of the synoptic-scale eddies in the initial conditions leads to a failure in reproducing the negative PNA pattern.

We can assume that when the synoptic-scale eddies are removed from the initial conditions there follow several days, which are critical to the genesis of the PNA, during which the high-frequency eddy activity is seriously deficient. As indicated by Kushnir and Wallace (1989), the high-frequency variability in such forecasts returns to normal amplitude after about one week. Our results imply that in the present model the genesis of a negative PNA relies more on the high-frequency transient activity than the genesis of a positive PNA. It is known from previous work (Lin and Derome, 1996, 1997) that the transient activity is weaker during a positive PNA than during a negative PNA over the North Pacific, at least during mean-seasonal PNAs. One important process that can be linked to the weak transient activity over the North Pacific during positive PNAs is the presence of the strong Aleutian low which tends to keep the baroclinic synoptic-scale eddies moving along its southern side, resulting in weak eddy activity over the North Pacific. During a negative PNA, on the other hand, the large-scale anticyclonic flow in the North Pacific tends to guide the transients northward, leading to strong eddy activity. The transients, however, are not passive participants in this process, but interact with and feedback onto the low-frequency flow, in such a way that it is difficult to assess cause and effect. The coexistence of the low-frequency PNA flow and the high-frequency eddies may well indicate that they depend on each other. The existence of a negative PNA may require a higher level of transient activity in the North Pacific than that of a positive one. In the first a few days of the forecast experiments, the development of the baroclinic eddies may be sufficient to support the onset of a positive PNA, but not to generate a negative PNA.

The removal of the high-frequency transients in the initial conditions introduces a considerable amount of error into the forecasts. The rms of the 500 hPa geopotential height error is calculated as:

$$E_{\mathrm{rms}} = \left(\frac{1}{N-1} \sum_{i=1}^{N} (Z_{\mathrm{f}} - Z_{\mathrm{c}})^2 \right)^{1/2}, \tag{5}$$

where Z_{f} is the forecast geopotential height at 500 hPa and Z_{c} is the corresponding geopotential height for the control run, N is the number of experiments, i.e, $N = 100$ and 118 for the positive and negative PNA experiments, respectively. The distributions of rms error of the 500 hPa geopotential height at the initial states for the positive and negative PNA forecast experiments shown in Figs. 5a, b, respectively, are seen to have similar patterns and magnitudes. Both have high rms errors in the midlatitude storm track regions with a maximum of about 90 m in the North Pacific, reflecting the removal of the baroclinic transients. Figs. 6a, b show the distributions of rms error averaged over days 6 to 10 after the integration for the positive and negative PNA runs, respectively. For the forecast of the positive PNA (Fig. 6a), we see just a small increase of error near the west coast of North America. The maximum rms error has reached 120 m at this time, about 30 m above that in the initial state. On the other hand, the error grows fast in the Pacific–North American region for the forecast of the negative PNA (Fig. 6b). The rms error centre over the North Pacific is about 240 m, double of its counterpart in the case of the positive PNA. The pattern of the error field, with its three centres, reflects the failure in forecasting the onset of the negative PNA.

5. Conclusion

A perpetual winter run of a 3-level Q–G model has been analyzed to study the time evolution of onsets of persistent positive and negative PNA anomalies, and their predictability. Special emphasis has been placed on the role of the synoptic-scale transients.

Through the composites of 100 positive and 118 negative PNA cases, it was shown that five days before the onset of a positive PNA anomaly there is signature of a negative PNA anomaly with a negative height anomaly over western Canada. On the other hand, 5 days before the onset of a negative PNA, a significant positive height anomaly is observed over western Canada. In both cases, the height anomaly over Canada moves southwestward and stops over the North Pacific. It then intensifies and a wave train develops downstream. The evolution of the anomaly pattern downstream from the central Pacific qualitatively resembles that observed in simple time-dependent models of horizontal kinetic energy dispersion on a sphere from a quasi-stationary vorticity source (Hoskins et al., 1977), indicating that this is an important process for the downstream development of the model's PNA anomalies.

To examine the role played by the synoptic-scale transients, prediction experiments starting from day -5 (5 days before the appearance of a PNA anomaly) were conducted, in which the synoptic-scale transients were removed by a 5-day average centred at day -5. The results show that even without these transients in the initial conditions, the onset process of a positive PNA anomaly can be reproduced quite well. On the other hand, the onset of a negative PNA cannot be predicted if the synoptic-scale transients are absent from the initial conditions.

Our results indicate that the sensitivity of the low-frequency flow to the initial specification of the high-frequency component of the field is a)

b)

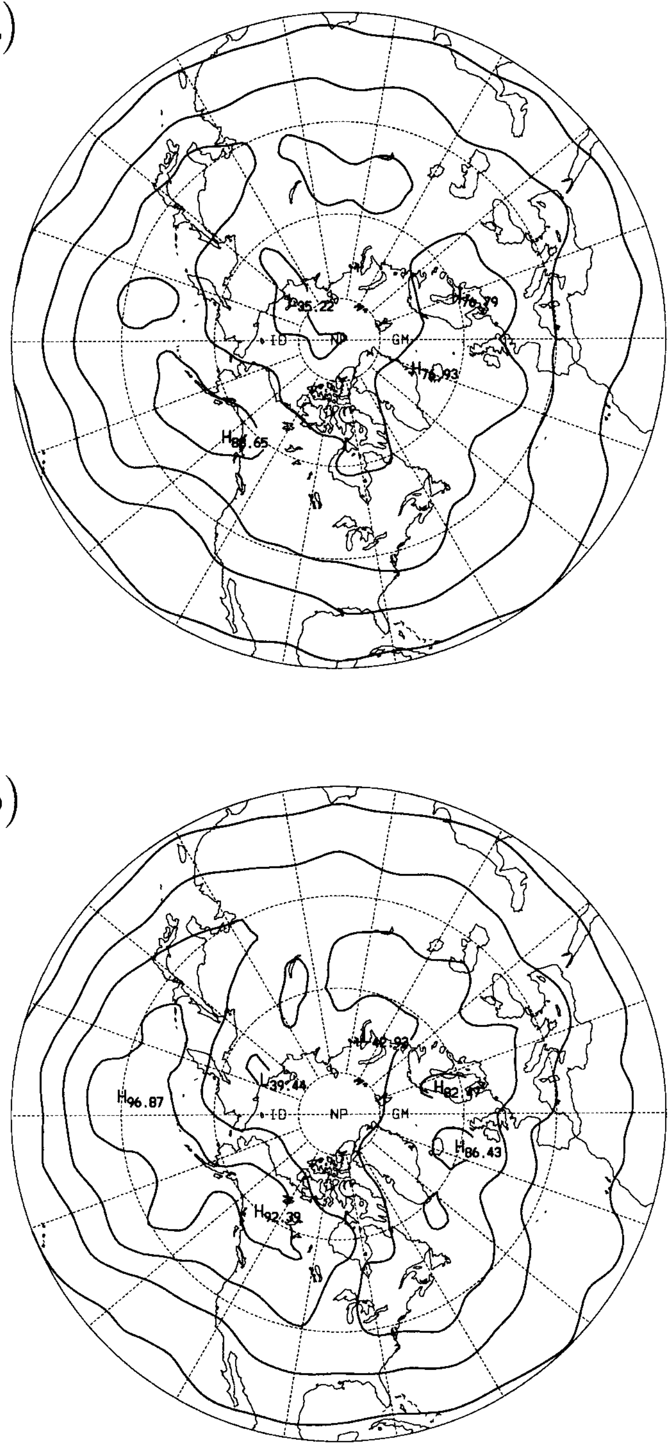

Fig. 5. Initial height rms error at 500 hPa for (a) positive PNA runs; (b) negative PNA runs. Contour interval is 20 m.

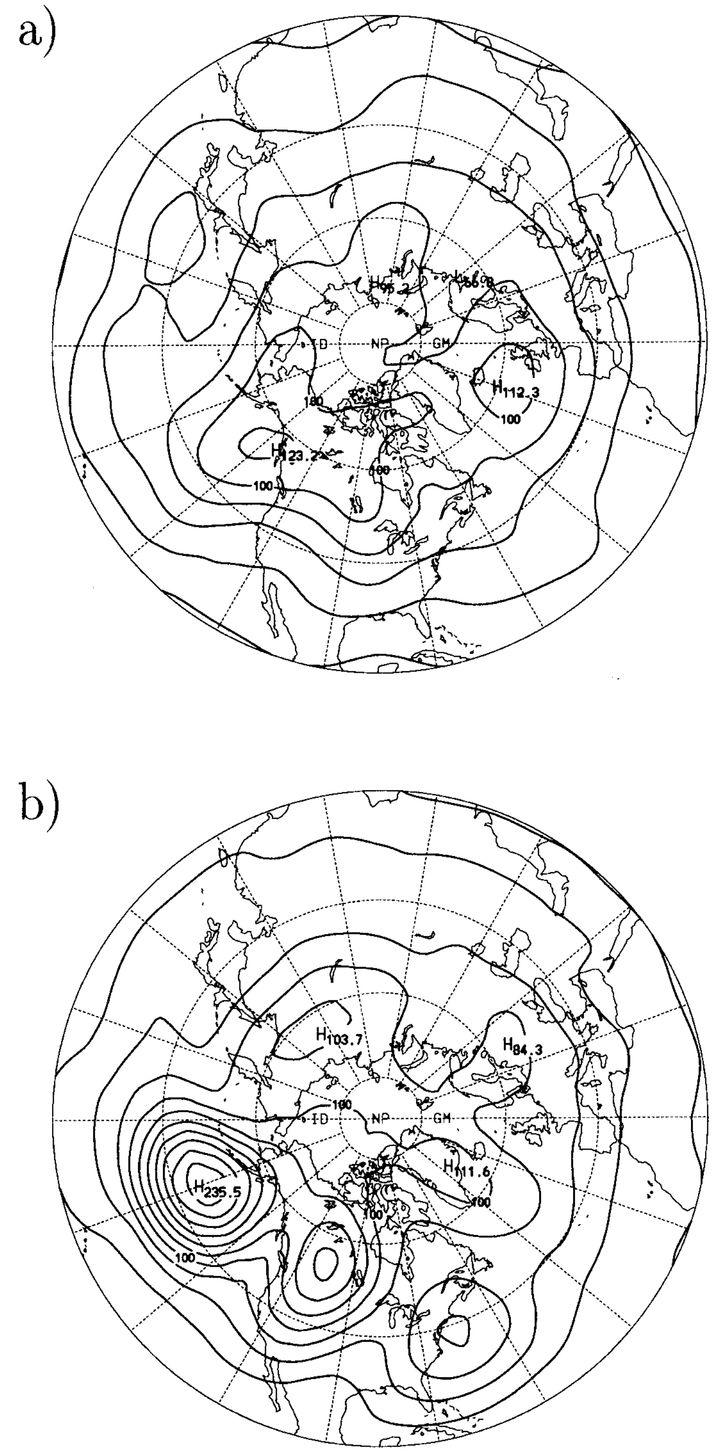

Fig. 6. rms error averaged over day 6 to 10 for (a) positive PNA runs; (b) negative PNA runs. Contour interval is 20 m.

regime-dependent. It would be of interest to see whether this dependence is also present in the more complex models used for long-range (including seasonal) predictions. If that is the case, an a priori knowledge of the dependence could have pratical value in predicting the forecast skill.

From the prediction experiments of the negative PNA, we saw that the removal of high-frequency transients leads to a possible development of another atmospheric low-frequency mode — the WP pattern. The link between the transition of modes and the role played by the synoptic-scale eddies is of great interest and is worth further investigations.

6. Acknowledgements

This research was supported by research grants from the Natural Sciences and Engineering Research Council and the Atmospheric Environment Service of Canada.

REFERENCES

Corti, S. and Palmer, T. N. 1997. Sensitivity analysis of atmospheric low-frequency variability. *Q. J. Roy. Meteor. Soc.* **123**, 2425–2447.

Dole, R. M. and Gordon, N. D. 1983. Persistent anomalies of the extratropical Northern Hemisphere wintertime circulation: Geophysical distribution and regional persisnence characteristics. *Mon. Wea. Rev.* **111**, 1567–1586.

Dole, R. M. 1986. The life cycles of persistent anomalies and blocking over the North Pacific. *Adv. in Geophysics* **29**, 31–69.

Frederiksen, J. S. 1979. The effect of long planetary waves on the regions of cyclogenesis. *J. Atmos. Sci.* **36**, 195–204.

Green, J. S. A. 1977. The weather during July 1976: Some dynamical considerations of the drought. *Weather* **32**, 120–126.

Hoskins, B. J., Simmons, A. J. and Andrews, D. G. 1977. Energy dispersion in a barotropic atmosphere. *Q. J. Roy. Meteor. Soc.* **103**, 553–567.

Horel, J. D. and Wallace, J. M. 1981. Planetary scale atmospheric phenomena associated with the Southern Oscillation. *Mon. Wea. Rev.* **109**, 813–829.

Klasa, M., Derome, J. and Sheng, J. 1992. On the interaction between the synoptic-scale eddies and the PNA teleconnection pattern. *Beitr. Phys. Atmosph./Contrib. Atmos. Phys.* **65**, 211–222.

Kushnir, Y. and Wallace, J. M. 1989. Interaction of low- and high-frequency transients in forecast experiment with a general circulation model. *J. Atmos. Sci.* **46**, 1411–1418.

Lin, H. and Derome, J. 1996. Changes in predictability associated with the PNA pattern. *Tellus* **48A**, 553–571.

Lin, H. and Derome, J. 1997. On the modification of the high- and low-frequency eddies associated with the PNA anomaly: an observational study. *Tellus* **49A**, 87–99.

Marshall, J. and Molteni, F. 1993. Toward a dynamical understanding of planetary-scale flow regimes. *J. Atmos. Sci.* **50**, 1792–1818.

Mullen, S. L. 1987. Transient eddy forcing of blocking flows. *J. Atmos. Sci.* **44**, 3–22.

Pandolfo, L. 1993. Observational aspects of the low-frequency intraseasonal variability of the atmosphere in middle latitudes. *Adv. Geophys.* **34**, 93–174.

Roads, J. O. 1987. Predictability in the extended range. *J. Atmos. Sci.* **44**. 3495–3527.

Simmons, A. J., Wallace, J. M. and Branstator, G. W. 1983. Barotropic wave propagation and instability, and atmospheric teleconnection patterns. *J. Atmos. Sci.* **40**, 1363–1392.

Wallace, J. M. and Gutzler, D. S. 1981. Teleconnections in the geopotential height field during the Northern Hemisphere winter. *Mon. Wea. Rev.* **109**, 784–812.